Force–conductance correlation in individual molecular junctions

Force–conductance correlation in individual molecular junctions

C Nef[1]**, P L T M Frederix**[2,3]**, J Brunner**[1]**, C Schönenberger**[1] **and M Calame**[1]

[1] Department of Physics, University of Basel, Klingelbergstrasse 82, CH-4056 Basel, Switzerland
[2] C-CINA, Biozentrum, University of Basel, Mattenstrasse 26, CH-4058 Basel, Switzerland

E-mail: Michel.Calame@unibas.ch

Abstract
Conducting atomic force microscopy is an attractive approach enabling the correlation of mechanical and electrical properties in individual molecular junctions. Here we report on measurements of gold–gold and gold–octanedithiol–gold junctions. We introduce two-dimensional histograms in the form of scatter plots to better analyze the correlation between force and conductance. In this representation, the junction-forming octanedithiol compounds lead to a very clear step in the force–conductance data, which is not observed for control monothiol compounds. The conductance found for octanedithiols is in agreement with the idea that junction conductance is dominated by a single molecule.

S Online supplementary data available from stacks.iop.org/Nano/23/365201/mmedia

(Some figures may appear in colour only in the online journal)

1. Introduction

In the last decade, new sophisticated tools have opened the possibility to fabricate atomic-scale metal terminals and to contact single molecules to measure their electrical properties. These tools include mechanical and electromigrated break junctions (BJs), scanning tunneling microscopy (STM) and atomic force microscopy (AFM) [1–4]. A molecular junction (MJ) constituted by two atomic contacts and bridged by a single or a few molecules does not form a rigid system, in particular at room temperature. A major challenge consists therefore in understanding and optimizing the arrangement of stable and reproducible contacts. It is known that, for a given molecule, different electrical conductance values can be observed in MJs. This has been attributed to different molecular conformations [5, 6], contact natures, adsorption sites and geometries [7, 6, 8–10] or microscopical arrangements of a few molecules in the junction [11–13]. To gain further insight, it is therefore important to assess the effect of contact geometry and mechanical strain on the conductance of an MJ. Conducting atomic force microscopy

(C-AFM) [14–16] represents an attractive approach for this purpose due to its ability to measure both electrical current and forces in parallel. Previous studies showed that the positions of force peaks appear correlated with conductance plateaus [14] during the formation of MJs and that force modulations influence the conductance as well as the contact stability [17, 18]. Furthermore, the influence of binding groups [14, 19, 17] and the molecular backbone [16] were investigated.

The aim of the present work is to shed more light on the mechanical and electrical properties of few gold atom and molecule junctions as well as on their differences. Therefore we use a break junction method where a conducting AFM tip is first moved into contact with a substrate and then slowly retracted. Covering the substrate with a self-assembled monolayer of thiolated alkanes (SAM) also allows investigations on few molecule contacts. We performed measurements on gold–gold contacts and gold–molecule–gold contacts with octanemonothiol (C8S) and octanedithiol (S8S). We show a novel and useful data representation in the form of two-dimensional histograms to underpin the correlation between electrical conductance and force in these junctions. Such plots are favored over simple

[3] Present address: Nanosurf AG, Gräubernstrasse 12-14, 4410 Liestal, Switzerland.

histograms because they contain more information and allow a more complete characterization of the mechanics involved, emphasizing the differences between atomic and molecular junctions. Our data support a dynamic scenario for the formation of molecular junctions which involves movement of the molecules on the contact electrode.

2. Experimental details

The experiments were carried out at room temperature on a commercial instrument (NanoWizard I, JPK Instruments, Berlin, Germany), equipped with a 100 μm x and y closed-loop scanner. A Au-coated Si wafer represents the first electrode. This substrate is functionalized with a SAM, containing C8S to prevent a contamination of the Au surface by the environment. To measure MJs, S8S was added, as it is expected to bridge the electrodes. The second electrode is a Au-coated Si cantilever (nominal force constant ≈ 4 N m^{-1}) also passivated with a C8S SAM. The gold coating is done by e-beam evaporation of a 10 nm Ti adhesion layer followed by a 100 nm thick Au layer at a rate of 1 Å s^{-1}. To protect the freshly coated surface from contamination, the samples and cantilevers were immediately immersed into the functionalizing solution. This solution contains 58 mM C8S in ethanol for the measurements of gold–gold contacts (for passivation) and the C8S experiments and 55 mM C8S and 3 mM S8S for the S8S measurements. The S8S molecules were used as received from Sigma-Aldrich; the C8S molecules were distilled before use. The samples were kept in this solution until the measurements were performed, typically between 12 and 72 h. Before immersing the samples in mesitylene, wherein the measurements were made, the samples were rinsed with ethanol thoroughly. The surface of our substrate is relatively rough (root mean square of 1.6 nm over an area of 1 μm^2) and has a grain size of ≈ 10–20 nm, thus we do not expect a full, homogeneous coverage of the SAM [20].

A schematic drawing of our setup is shown in figure 1(a). During a measurement, the cantilever is pushed towards the substrate with a velocity of ≈ 200 nm s^{-1} until a maximum force of 150 nN for the gold–gold and 15 nN for the gold–S8S–gold contacts is reached. A smaller force for the molecule measurements is used to protect the SAM from a harsh reorganization. The maximum force is maintained for 2 s. Then the cantilever is retracted at a speed of ≈ 15 nm s^{-1}, allowing the formation of few atom or molecule junctions. During the retraction, the force F between the probe and the sample is measured by multiplying the deflection signal V_F of a laser beam focused on the backside of the cantilever with the deflection sensitivity (DS) and the force constant k_c of the cantilever. The deflection sensitivity DS is obtained from the linear regime of a force–distance curve and k_c is determined using the thermal noise method implemented in the AFM system [21]. Simultaneously, the current I through the tip–sample contact is measured with a home-built amplifier and the conductance $G_{\text{tip–sample}}$ can be calculated by $G_{\text{tip–sample}} = I/(V_b - IR_s)$, where V_b is the applied bias voltage. The series resistor R_s limits the
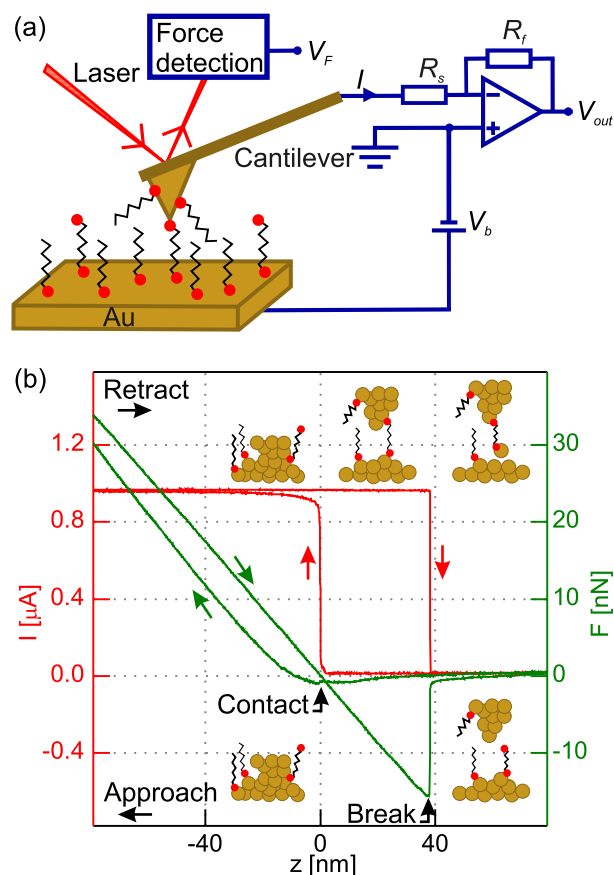

Figure 1. (a) Schematic drawing of the C-AFM setup and amplifier. Both the sample and the cantilever are gold coated and functionalized with a SAM. The series resistor R_s has either $R_s = 13$ kΩ or $R_s = 1$ GΩ, depending on the conductance range, 0.1–$10 G_0$ or 10^{-6}–$10^{-4} G_0$ respectively. (b) Contact formation and rupture in a schematic representation and corresponding force (green) and current (red) curves. The horizontal axis shows the piezo displacement. The mechanical and the electrical contact form at the same displacement. Note that in the subsequent figures we reverse the sign convention and represent the force in the breaking region with a positive sign.

current flowing through the junction and is needed to prevent the formation of shorts during full contact. This resistor is adjusted depending on the conductance range (13 kΩ for $(0.1$–$10 G_0)$ and 1 GΩ for $(10^{-6}$–$10^{-4} G_0)$). The bias voltage applied was $V_b = 50$ mV for the gold junctions and $V_b = 100$ mV for the MJs. Typical currents for gold–gold and gold–molecule–gold junctions were in the range of 4–5 μA and 100 pA respectively, where the detection limits are 0.3 μA and 0.8 pA.

A typical measurement curve is shown in figure 1(b). The zero of the piezo displacement in the z direction is defined as the point where the cantilever touches the surface while not being bent, which corresponds to zero force. We now describe the data in more detail, starting with the approach curves for current (red) and force (green). As long as no contact between tip and sample is established ($z > 0$ nm), the current and the force are below the detection limit. At $z \approx 20$ nm before the contact point, a small dip can be observed in the force curve. We attribute this dip to electrostatic forces
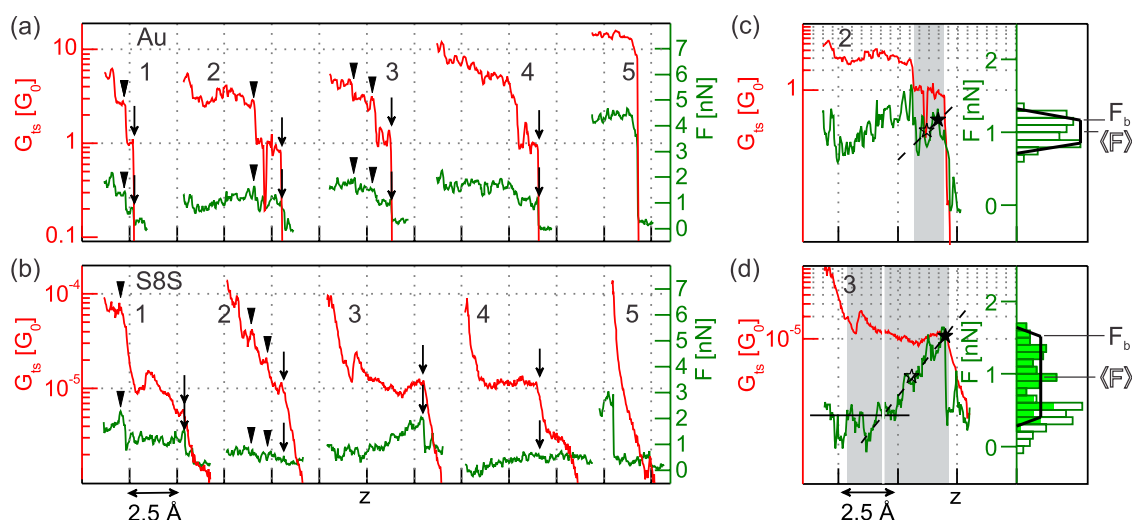
Figure 2. (a) Region of interest for typical retraction curves observed on gold samples passivated with a C8S SAM. The tip was pushed on the surface with a maximum force of 150 nN. (b) Characteristic curves of samples covered by an S8S SAM. The maximum pushing force was 15 nN to avoid large disturbances in the SAM. All measurements were made in mesitylene. For clarity the curves are separated from each other by an offset in the z-direction. In both figures, the z-axis ticks are separated by 2.5 Å. Plateaus at multiples of a certain conductance ($G_0 = \frac{2e^2}{h}$ for (a) and $G_{mol} = 1.1 \times 10^{-5} G_0$ for (b)) occurring coincidentally with jumps in the force curves are marked with arrows and arrowheads (multiples). (c) Details of curve 2 from (a) and (d) details of curve 3 from (b). We observe that the slope of the force curves is consistent with the actual force constant k_c of the cantilever (dashed black lines, $k_c = 3.2$ N m^{-1} in (c) and $k_c = 4.2$ N m^{-1} in (d)). The black line is horizontal. Gray areas emphasize the distance intervals corresponding to the last conductance plateau. On the right, histograms show the force distribution during the last conductance plateau (42 points for (c) and 139 points for (d)). The solid line shows an idealized force distribution for the linearly increasing force regime. The empty stars ☆ show the position of the mean force $\langle F \rangle$ and the full stars ★ show the position of the breaking force F_b.

between tip and sample, possibly caused by the bias voltage applied ($V_b = 10$ mV here). After the contact is established, the force increases linearly with the piezo displacement z and the current jumps to saturation. In this region a gold–gold contact consisting of multiple atoms is established between tip and sample, as schematically depicted by the drawing in the figure. Once the preset maximum force is reached, the cantilever is paused for two seconds and then retracted. A linear force–distance behavior develops again and extends to negative force values due to the adhesion between tip and sample until the contact is broken. During the retraction, the contact narrows until only a small number of atoms or even a single atom forms the bridge. Before the contact is broken, molecules present at the metal surfaces can bridge the electrodes by forming covalent bonds and thus establish a molecular junction. When both electrodes finally come apart, the force and current jump back to zero.

Because of microscopic structural rearrangements, no contact is like the previous one in atomic and molecular junctions. Large datasets are therefore needed to provide sufficient statistics. We collected between 1000 and 2000 curves at five or more different positions on the substrate per measurement series. A home-written data filtering program based on previous work [22] is used for curve processing. Typically 10–20% of the curves pass the filter and are used for further analysis. Details of the algorithm are provided in the supporting information available at stacks.iop.org/Nano/23/365201/mmedia. This system ensures that no systematic bias influences the data through manual selection.

3. Results and discussion

Representative retraction force $F(z)$ and tip–sample conductance $G_{ts}(z)$ curves for gold and S8S samples are shown for the regions of interest in figures 2(a) and (b) respectively. In figure 2(a) the conductance curves $G_{ts}(z)$ show plateaus at multiples of $G_0 = \frac{2e^2}{h}$. At the position where a conductance plateau breaks, the force curve increases linearly to finish with an abrupt drop corresponding to the end of the conductance plateau. This leads to a sawtooth-like shape for the force curves. Most curves (1–4) show forces between 1 and 2 nN. Curve 5 is an example where no clear plateaus can be observed. Here the maximum conductance is higher ($> 10 G_0$), which means that a larger contact area is present. As a consequence, the forces reach higher values (≈ 4.5 nN) as well. If the contact area remains large during retraction, the cantilever can accumulate more elastic energy. As a consequence, when the contact breaks without a step-wise narrowing of the tip–substrate constriction, larger maximal forces appear in the breaking process [23, 1]. For each curve, the position of the last conductance plateau appearing at G_0 is indicated by a vertical arrow, showing its final z-coordinate before breaking. This corresponds to the situation where the Au bridge is composed of a single Au atom in width [24]. Plateaus appearing at larger conductance values are indicated by arrowheads. Figure 2(c) focuses on the second curve in figure 2(a). The average slope of the force curve $F(z)$ during a conductance plateau (shaded gray area) corresponds to the calibrated force constant of the cantilever $k_c = 3.2$ N m^{-1} for this experiment (dashed black line). This means that, upon

retraction, the tip–sample-separation (TSS) stays constant and only the cantilever is bent. The right panel shows the force distribution for $F(z)$ during the last conductance plateau at $1\,G_0$. For a noiseless, linearly increasing force–distance curve, the distribution should be flat. The noise in the curve leads to a trapezoidal shape for the distribution, as shown by the solid line in figure 2(c). The counts enclosed by the solid line are equivalent to the counts in the histogram. The distribution is symmetric around the mean force, which is denoted by $\langle F \rangle$. An open star symbol (☆) shows its position along the force trace $F(z)$. The breaking force F_b corresponds to the maximum force reached immediately before a sharp drop in conductance and is observed at the end of the last conductance plateau. F_b is indicated by a solid star symbol (★) in the conductance trace. We denote the breaking force as the maximum force minus the standard deviation (sd) of the force noise along the conductance plateau. For this particular curve we obtain $F_b \approx 1.2$ nN for a gold–gold contact, slightly below the 1.4 nN [16] and 1.5 nN [25, 26] found in earlier experiments and slightly above the calculated forces of 0.9 nN [27] and 1.1 nN [28]. Note that this is the breaking force obtained from a single $F(z)$ curve. In the discussion of figure 4 below, we will provide a statistical analysis over ensembles of conductance and force traces.

In the presence of dithiolated molecules (figure 2(b)), a last conductance plateau is observed at $G_{ts} = G_{mol} \approx 1.1 \times 10^{-5}\,G_0$. Features at lower conductance values are not statistically relevant, as will be shown when discussing the histograms for the whole dataset. This plateau is assumed to correspond to the situation where the contact to the last molecule bridging the electrodes breaks and we can interpret the conductance G_{mol} as representative of an MJ where transport is dominated by a single molecule [29]. The conductance thus obtained for octanedithiol is in good agreement with previously reported values [30, 31, 12, 32]. Curve 5 in figure 2(b) is an example where no plateaus appear in that conductance regime and corresponds to the case where no molecular junction is formed. This occurs in about 40% of the curves. If we now focus on the force traces, we observe that, except for curve 3, the slope is smaller than the calibrated force constant of the cantilever $k_c = 4.2$ N m^{-1} and no clear jumps are observed. It is known that a breakdown of the junctions can occur spontaneously at room temperature [33], without the application of an external force. This seems to be the case for most of the measured curves. However, we also note that, for about 20% of the conductance curves showing conductance plateaus, the force is first constant (on average) and then rises linearly until it drops at the position corresponding to the end of the conductance plateau. Curve 3 in figure 2(b) is representative of this scheme. Additional force traces showing a similar behavior are provided in the supporting information (available at stacks.iop.org/Nano/23/365201/mmedia). We consider this behavior further with figure 2(d), which shows a detailed view of curve 3. The extension of the last conductance plateau is emphasized by a gray shaded area. In the corresponding force curve, the vertical line shows the limit between a
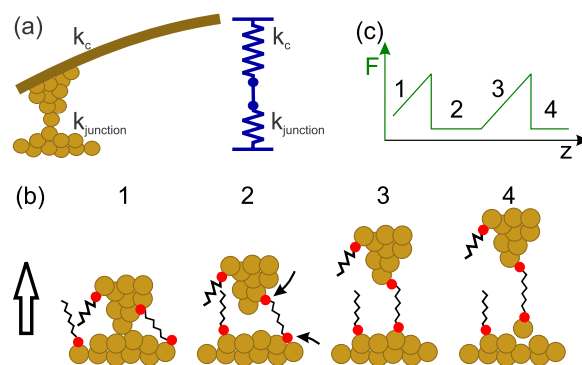

Figure 3. (a) Spring model for the cantilever and the contact. (b) Proposed dynamic mechanism for molecular contact formation. 1. The tip is still in contact with the sample but a molecule is already covalently bound to both electrodes. 2. After the gold–gold contact has been broken, the molecule is not necessarily aligned perpendicular to the surface and at the narrowest position. 3. When the cantilever is retracted the molecule is pulled upright and moves to the middle of the junction. 4. If the force applied to the junction becomes too large, the contact breaks. (c) Schematic force curve, corresponding to the steps described in (b).

regime where the force remains constant on average (solid line) and a regime where it increases linearly (dashed line). Remarkably, the slope in the linear regime corresponds to the cantilever force constant k_c (dashed line), which was $k_c = 4.2$ N m^{-1} in this measurement. The mean force constant in the linear regime obtained from a fit to the data is $k_c = 4.1 \pm 0.2$ N m^{-1} (see supporting information available at stacks.iop.org/Nano/23/365201/mmedia). The force histogram (right panel) was obtained from the force trace in the distance interval corresponding to the conductance plateau. The constant force region leads to a large force peak close to zero, whereas the linearly increasing regime (solid histogram) leads to a trapezoidal force distribution. In analogy to the analysis done for gold–gold contacts, we deduce a mean force (☆) and breaking force (★) from the linearly increasing regime of the $F(z)$ trace. We obtain in this case a breaking force $F_b \approx 1.5$ nN, close to the value observed for Au–Au contacts.

To gain further insight in the mechanics of junction formation, we can look at the setup as a simple series connection of two springs (figure 3). The first spring is the cantilever with a spring constant k_c; the second spring k_j represents either the atomic gold–gold contact or the molecular junction (Au contact–molecule–Au contact). In the following discussion, we focus on molecular junctions. The general case where the slope of the force trace is smaller than k_c is difficult to assess given the large number of possible microscopic arrangements. However, for force traces such as that shown in figure 2(d), the situation is more favorable: we propose that a rearrangement of the molecule takes place during the pulling of the cantilever, as depicted in figure 3(b). A corresponding schematic force trace is shown in figure 3(c). At point 1 the tip is still in contact with the sample, while molecules can already bind covalently to both electrodes [34]. When the gold bond breaks, the molecule is not necessarily fully stretched in the junction and the force will decrease: we enter regime
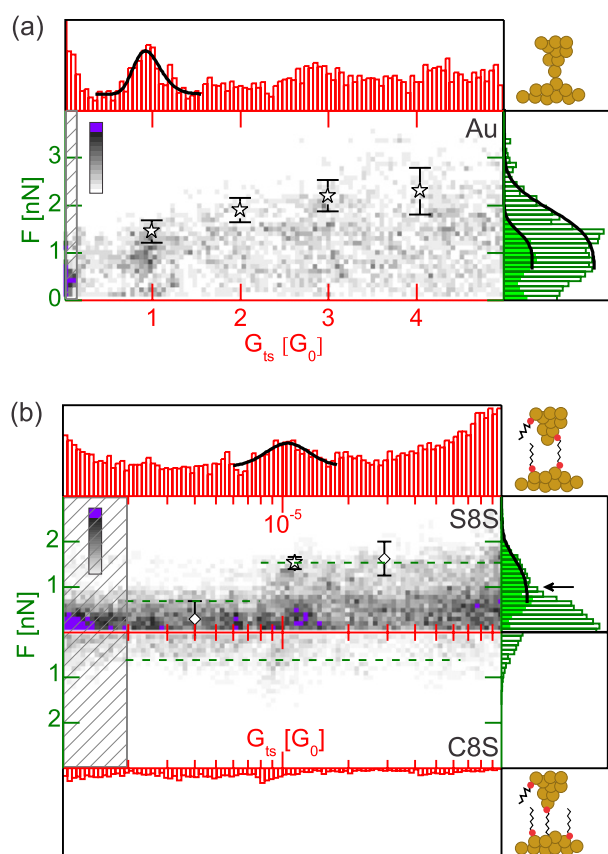
Figure 4. Two-dimensional normalized histograms (scatter plots) providing an overview over tip–sample conductance G_{ts} and force F for (a) gold–gold (194 curves) and (b) gold–octanedithiol–gold (upper panel, 115 curves) as well as gold–octanemonothiol–gold (lower panel, 114 curves) contacts. Note that the data for alkane monothiols (C8S) are mirrored for easier comparison. For each two-dimensional histogram, we show the conductance (top panel) and force (right panel) 1D normalized histograms corresponding respectively to the full conductance and force ranges. The crosshatched regions indicate the noise limit and are excluded from 1D force histograms. In (a), the open star symbols show the mean breaking force $\overline{F_b}$ for conductance intervals extending $\pm 0.5\, G_0$ around multiples of G_0. The open stars are plotted at the mean conductance over each conductance interval. The 1D force histogram corresponding to the first conductance interval is shown with solid bars. In (b), the diamond symbols show the mean force value over the conductance intervals $2 \times 10^{-6}\, G_0$–$8 \times 10^{-6}\, G_0$ and $\overline{F_b}$ for the interval $8 \times 10^{-6}\, G_0$–$10^{-4}\, G_0$. The open star symbol shows $\overline{F_b}$ for the interval $8 \times 10^{-6}\, G_0$–$1.6 \times 10^{-5}\, G_0$, plotted at the mean conductance value over the interval. The 1D force histogram obtained by subtracting the normalized force histograms corresponding to the upper and lower conductance ranges is shown in solid bars.

2. As the cantilever is further retracted, the molecule will migrate and align itself between the Au contacts. Based on our data, we speculate that the migration process does not require a substantial force. At room temperature the surface gold atoms are mobile: Au-bound molecules without a strong local molecular ordering will therefore also be mobile. Upon stretching, we can thus anticipate a migration of the molecules to the narrowest part of the junction without the need for a substantial extra mechanical force. This scenario is also supported by recent calculations showing the high mobility

of a molecular phase adsorbed on Au atomic contacts due to the fluctuations of the atomic positions in the narrowest part of the contact [35]. In this regime, any unstretched molecule will act as a very soft spring. Once the narrowest position between electrodes is reached, the molecule will fully extend and a further retraction of the cantilever lead to a linear increase of the force (3). We observe that the slope corresponds to k_c. This means that the junction composed by the metal contacts and the stretched molecule is now behaving as a stiffer spring than the cantilever. Once the breaking force is reached, the cantilever separates from the substrate and the force goes back to zero (4).

We now turn to a statistical analysis and investigate the correlation between force and conductance. While simple histograms built from individual curves give a useful overview, they do not show how force and conductance relate to each other during the breaking of a molecular junction. The two-dimensional histograms (scatter plots) in figure 4 help visualizing this interplay. The figure gives an overview over conductance and force properties for gold–gold (figure 4(a), 194 curves) as well as gold–molecule–gold contacts (figure 4(b); upper panel, gold–octanedithiol–gold, 115 curves; lower panel, gold–octanemonothiol–gold, 114 curves). In these histograms, we concentrate on the stretching regime, which means that only conductance points with a corresponding positive force are represented. For the gold–molecule–gold junction data in figure 4(b) a logarithmic scale helps to better visualize the conductance peaks [36]. The top and right panels show conductance and force histograms respectively. A detailed description of the two-dimensional histogram generation and an example for a single curve are provided in the supporting information (available at stacks. iop.org/Nano/23/365201/mmedia).

We first focus on the data for gold–gold contacts in figure 4(a). The data show a clear cluster in the scatter plot and a peak in the conductance histogram (top panel) at $\approx 0.95\, G_0$ (mean of a Gaussian fit to a log-normal distribution [37]). The value is slightly lower than the conductance quantum $1\, G_0$, which can be attributed to a small resistance in series arising from wires and contacts [38, 1]. While less clear than at $1\, G_0$, a clustering around ≈ 2 and $3\, G_0$ can still be seen, arising from the conductance plateaus visible in the individual conductance traces (figure 2). The force histogram on the right panel (open bars) includes all forces corresponding to data points with a conductance between $0.25\, G_0$ and $5\, G_0$. The second force histogram (solid bars) corresponds to a conductance range extending from $0.5\, G_0$ to $1.5\, G_0$, where atomic contacts with a single Au atom are formed. The crosshatched region to the left of the scatter plot is not taken into account for the force histograms. The threshold corresponds to the conductance noise level. To find the average breaking force $\overline{F_b}$ from a scatter plot built using an ensemble of force traces, we proceed as follows. We emphasized previously that an ideal (noiseless) force curve leads to a flat force distribution: this results in a rectangular histogram with a maximum force corresponding to F_b. The number of counts (height) of the histogram depends on the sampling rate and the slope of the force curve. We assume a

constant slope over the whole dataset here. Successive force curves will result in a normal distribution of F_b values. The shape of the histogram including all force traces will therefore correspond to the integral of a Gaussian distribution (see supporting information available at stacks.iop.org/Nano/23/365201/mmedia). Corresponding fits to the upper flank of the force histograms for the overall ($0.25\,G_0$–$5\,G_0$) and plateau ($0.5\,G_0$–$1.5\,G_0$) regions are shown in figure 4(a). The open star symbols in the scatter plot indicate the position of the mean breaking force $\overline{F_b}$ plotted at the mean conductance value for conductance intervals of $\pm 0.5\,G_0$ around integer values of G_{ts}/G_0 and the error bars correspond to the standard deviation (see supporting information available at stacks.iop.org/Nano/23/365201/mmedia for the corresponding histograms and fits). We note that the spread of forces around $\overline{F_b}$ broadens with increasing conductance while $\overline{F_b}$ itself only grows slightly. This is expected: when more atoms contribute to the contact, larger forces can appear. From the scatter plot and the corresponding force histogram, we can thus estimate the average breaking force $\overline{F_b}$ more easily than by analyzing all individual traces. Using the procedure described above and for the force histogram corresponding to conductances ranging between $0.5\,G_0$ and $1.5\,G_0$, we obtain $F_b = 1.45 \pm 0.23$ nN, in good agreement with values reported experimentally for gold–gold contacts [25, 26, 16].

Figure 4(b) shows a scatter plot for octanedithiols (S8S, upper panel) as well as control measurements with only octanemonothiols (C8S, lower panel) together with the corresponding conductance and force histograms. The conductance histograms, force histograms and scatter plots are normalized to the number of data curves and shown at the same scale. We first consider the data for octanedithiols (S8S) in the upper part of the figure. A clear peak in the conductance histogram (top panel) can be seen close to $10^{-5}\,G_0$, which corresponds to the last conductance plateau observed in individual conductance traces. A fit to a log-normal distribution [37] provides a conductance $G_{ts} \approx G_{mol} = 1.1 \times 10^{-5}\,G_0$, which we interpret as a characteristic value for the molecular junction. The force histogram built from the data over the whole conductance range above the noise threshold (open bars) does not however show a clear peak but rather a shoulder at around 1 nN. Looking at the scatter plot helps to better understand the correlation between force and conductance during the breaking of the junction. At low conductance values, the force mostly remains below 0.7 nN (dashed line). For conductance values larger than $\approx 0.8\,G_{mol}$, we clearly see that the maximum force can reach higher values, as emphasized by the second horizontal dashed line at 1.6 nN. This results in a shoulder in the force histogram (arrow). We attribute the higher force values above $\approx 0.8\,G_{mol}$ to the formation of MJs. The mean force in the background region (from $2 \times 10^{-6}\,G_0$–$8 \times 10^{-6}\,G_0$) is 0.3 ± 0.4 nN (open diamond). The second force histogram in the right panel (solid bars) is obtained by subtracting the histograms corresponding to the two conductance intervals: below and above $0.8\,G_{mol}$. Both histograms have been normalized to the number of conductance bins contributing before the subtraction. This histogram is fitted using the same procedure as described

above (solid line). The average breaking force above $0.8\,G_{mol}$ corresponds to 1.6 ± 0.4 nN (open diamond).

To estimate the junction breaking force, we restrict the analysis to the force data corresponding to the peak in conductance, i.e. $8 \times 10^{-6}\,G_0$–$1.6 \times 10^{-5}\,G_0$. Performing this, we obtain an average breaking force $\overline{F_b} = 1.5 \pm 0.1$, which is very close to that obtained for the gold–gold junction. This further supports the hypothesis that the gold–gold bond is breaking in the MJs and not the sulfur–gold bond [7, 39, 33]. The force data for the MJs do not show a tendency for broadening as observed for gold–gold contacts. We also observe that the most probable conductance value of $G_{mol} = 1.1 \times 10^{-5}\,G_0$ is in remarkable agreement with the value of $1.2 \times 10^{-5}\,G_0$ attributed to a single S8S molecule junction in earlier work [12]. Should a few molecules bridge the gap simultaneously and equally contribute to the junction conductance, we would expect clear conductance plateaus at integer multiples of G_{mol}. Such plateaus are only rarely observed at a value of $G_{ts} = 2\,G_{mol}$ (see e.g. curve 2 in figure 2(b)). We infer from these observations that we mostly observe the breaking of individual molecules bound to both contact electrodes. This is also supported by the fact that we operate at a low gap opening speed and that due to thermal fluctuations a molecule–electrode dissociation can spontaneously happen [33], which lowers the probability to have a few molecules bridging the gap simultaneously.

We finally consider the lower panel where the monothiol (C8S) data are mirrored for easier comparison to the dithiol data. We observe here that the force mostly remains below 0.7 nN over the whole conductance range (dashed line), while the force histogram shows no shoulder. There is therefore no clear evidence for the formation of mechanically stable MJs in this conductance range. We observe that a small peak around $8 \times 10^{-6}\,G_0$ is visible in the conductance histogram, with the corresponding force data being slightly larger than the background. The force however does not reach the values observed in the presence of dithiols and the signal is weak. It has been proposed that molecular bridges may form due to an interdigitation of neighboring alkane chains [40]. We do not however think that this is a realistic scenario here. As compared to molecular junctions built from conjugated compounds where intermolecular interactions in the form of stacking effects have been reported [41–43], the Van der Waals interaction between neighboring thiolated alkane chains is substantially weaker.

4. Conclusions

In summary, we have investigated the formation and breaking of gold–gold and gold–molecule–gold junctions using a C-AFM, measuring electrical transport as well as mechanical properties simultaneously. We show that scatter plots (two-dimensional histograms) are a powerful method to analyze the data and correlate force and conductance. Using this representation, we can clearly identify the force–conductance region where molecular junctions are formed. We observe that gold–gold and gold–S8S–gold contacts break on average at a very similar force. This supports the assumption that the

gold–gold bond is the weakest point in alkanedithiol-based molecular contacts. We also showed that the mechanism of junction formation is a dynamic process, which can be probed by C-AFM. This is particularly striking in about 20% of the measurements, which support a scenario where the molecules can migrate along the metal contacts before the junction breaks, thanks to the mobility of surface atoms.

Acknowledgments

References

[1] Agraït N, Yeyati A L and van Ruitenbeek J M 2003 Quantum properties of atomic-sized conductors *Phys. Rep.* **377** 81–279

[2] Nichols R J, Haiss W, Higgins S J, Leary E, Martín S and Bethell D 2010 The experimental determination of the conductance of single molecules *Phys. Chem. Chem. Phys.* **12** 2801–15

[3] Chen F, Hihath J, Huang Z F, Li X L and Tao N J 2007 Measurement of single-molecule conductance *Annu. Rev. Phys. Chem.* **58** 535–64

[4] Osorio E A, Bjørnholm T, Lehn J-M, Ruben M and van der Zant H S J 2008 Single-molecule transport in three-terminal devices *J. Phys.: Condens. Matter* **20** 374121

[5] Haiss W, van Zalinge H, Bethell D, Ulstrup J, Schiffrin D J and Nichols R J 2006 Thermal gating of the single molecule conductance of alkanedithiols *Faraday Discuss.* **131** 253–64

[6] Li C, Pobelov I, Wandlowski T, Bagrets A, Arnold A and Evers F 2008 Charge transport in single Au | alkanedithiol | Au junctions: coordination geometries and conformational degrees of freedom *J. Am. Chem. Soc.* **130** 318–26

[7] Li X L, He J, Hihath J, Xu B Q, Lindsay S M and Tao N J 2006 Conductance of single alkanedithiols: conduction mechanism and effect of molecule–electrode contacts *J. Am. Chem. Soc.* **128** 2135–41

[8] Haiss W, Martín S, Leary E, van Zalinge H, Higgins S J, Bouffier L and Nichols R J 2009 Impact of junction formation method and surface roughness on single molecule conductance *J. Phys. Chem.* C **113** 5823–33

[9] von Wrochem F, Gao D, Scholz F, Nothofer H-G, Nelles G and Wessels J M 2010 Efficient electronic coupling and improved stability with dithiocarbamate-based molecular junctions *Nature Nanotechnol.* **5** 618–24

[10] Diez-Perez I, Hihath J, Hines T, Wang Z S, Zhou G, Müllen K and Tao N J 2011 Controlling single-molecule conductance through lateral coupling of π orbitals *Nature Nanotechnol.* **6** 226–31

[11] Magoga M and Joachim C 1999 Conductance of molecular wires connected or bonded in parallel *Phys. Rev.* B **59** 16011–21

[12] González M T, Brunner J, Huber R, Wu S M, Schönenberger C and Calame M 2008 Conductance values of alkanedithiol molecular junctions *New J. Phys.* **10** 065018

[13] Arroyo C R, Leary E, Castellanos-Gómez A, Rubino-Bollinger G, González M T and Agraït N 2011 Influence of binding groups on molecular junction formation *J. Am. Chem. Soc.* **133** 14213–9

[14] Xu B Q, Xiao X Y and Tao N J 2003 Measurements of single-molecule electromechanical properties *J. Am. Chem. Soc.* **125** 16164–5

[15] Chen F, Zhou J F, Chen G J and Xu B Q 2010 A novel highly integrated SPM system for single molecule studies *IEEE Sensors J.* **10** 485–91

[16] Frei M, Aradhya S V, Koentopp M, Hybertsen M S and Venkataraman L 2011 Mechanics and chemistry: single molecule bond rupture forces correlate with molecular backbone structure *Nano Lett.* **11** 1518–23

[17] Zhou J F, Chen G J and Xu B Q 2010 Probing the molecule-electrode interface of single-molecule junctions by controllable mechanical modulations *J. Phys. Chem.* C **114** 8587–92

[18] Franco I, George C B, Solomon G C, Schatz G C and Ratner M A 2011 Mechanically activated molecular switch through single-molecule pulling *J. Am. Chem. Soc.* **133** 2242–9

[19] Tsutsui M, Taniguchi M and Kawai T 2009 Quantitative evaluation of metal–molecule contact stability at the single-molecule level *J. Am. Chem. Soc.* **131** 10552–6

[20] Love J C, Estroff L A, Kriebel J K, Nuzzo R G and Whitesides G M 2005 Self-assembled monolayer of thiolates on metals as a form of nanotechnology *Chem. Rev.* **105** 1103–69

[21] Butt H-J and Jaschke M 1995 Calculation of thermal noise in atomic force microscopy *Nanotechnology* **6** 1–7

[22] Bosshart P D, Casagrande F, Frederix P L T M, Ratera M, Bippes C A, Müller D J, Palacin M, Engel A and Fotiadis D 2008 High-throughput single-molecule force spectroscopy for membrane proteins *Nanotechnology* **19** 384014

[23] Stalder A and Dürig U 1996 Study of plastic flow in ultra small Au contacts *J. Vac. Sci. Technol.* B **14** 1259–63

[24] Agraït N, Rodrigo J G and Vieira S 1993 Conductance steps and quantization in atomic-size contacts *Phys. Rev.* B **47** 12345–8

[25] Rubio G, Agraït N and Vieira S 1996 Atomic-sized metallic contacts: mechanical properties and electronic transport *Phys. Rev. Lett.* **76** 2302–5

[26] Rubio-Bollinger G, Bahn S R, Agraït N, Jacobsen K W and Vieira S 2001 Mechanical properties and formation mechanisms of a wire of single gold atoms *Phys. Rev. Lett.* **87** 026101

[27] Okamoto M and Takayanagi K 1999 Structure and conductance of a gold atomic chain *Phys. Rev.* B **60** 7808–11

[28] Sørensen M R, Brandbyge M and Jacobsen K W 1998 Mechanical deformation of atomic-scale metallic contacts: structure and mechanisms *Phys. Rev.* B **57** 3283–94

[29] Xu B Q and Tao N J 2003 Measurement of single-molecule resistance by repeated formation of molecular junctions *Science* **301** 1221–3

[30] Haiss W, Nichols R J, van Zalinge H, Higgins S J, Bethell D and Schiffrin D J 2004 Measurement of single molecule conductivity using the spontaneous formation of molecular wires *Phys. Chem. Chem. Phys.* **6** 4330–7

[31] Cui X D, Primak A, Zarate X, Tomfohr J, Sankey O F, Moore A L, Moore T A, Gust D, Harris G and Lindsay S M 2001 Reproducible measurement of single-molecule conductivity *Science* **294** 571–4

[32] Akkermann H B and de Boer B 2008 Electrical conduction through single molecules and self-assembled monolayers *J. Phys.: Condens. Matter* **20** 013001

[33] Huang Z F, Chen F, Bennett P A and Tao N J 2007 Single molecule junction formed via Au-thiol contact: stability and breakdown mechanism *J. Am. Chem. Soc.* **129** 13225–31

[34] Huisman E H, Trouwborst M L, Bakker F L, de Boer B, van Wees B J and van der Molen S J 2008 Stabilizing single atom contacts by molecular bridge formation *Nano Lett.* **8** 3381–5

[35] French W R, Iacovella C R and Cummings P T 2011 The influence of molecular adsorption on elongating gold nanowires *J. Phys. Chem.* C **115** 18422–33

[36] González M T, Wu S, Huber R, van der Molen S J, Schönenberger C and Calame M 2006 Electrical conductance of molecular junctions by a robust statistical analysis *Nano Lett.* **6** 2238–22342

[37] Huber R *et al* 2008 Electrical conductance of conjugated oligomers at the single molecule level *J. Am. Chem. Soc.* **130** 1080–4

[38] Brandbyge M, Schiøtz J, Sørensen M R, Stoltze P, Jacobsen K W, Nørskov J K, Olesen L, Laegsgaard E, Stensgaard I and Besenbacher F 1995 Quantized conductance in atom-sized wires between two metals *Phys. Rev.* B **52** 8499–514

[39] Krüger D, Fuchs H, Rousseau R, Marx D and Parrinello M 2002 Pulling monoatomic gold wires with single molecules: an *ab initio* simulation *Phys. Rev. Lett.* **89** 186402

[40] Huisman E 2010 Electron transport through single organic molecules and self-assembled monolayers *PhD Thesis* University of Groningen

[41] Wu S, González M T, Huber R, Grunder S, Mayor M, Schönenberger C and Calame M 2008 Molecular junctions based on aromatic coupling *Nature Nanotechnol.* **3** 569–74

[42] Martín S, Grace I, Bryce M R, Wang C, Jitchati R, Batsanov A S, Higgins S J, Lambert C J and Nichols R J 2010 Indentifying diversity in nanoscale electrical break junctions *J. Am. Chem. Soc.* **132** 9157–64

[43] González M T, Leary E, García R, Verma P, Herranz M Á, Rubio-Bollinger G, Martín N and Agraït N 2011 Break-junction experiments on acetyl-protected conjugated dithiols under different environmental conditions *J. Phys. Chem.* C **115** 17973–8